# Dalton Transactions

Accepted Manuscript






ROYAL SOCIETY OF CHEMISTRY

www.rsc.org/dalton

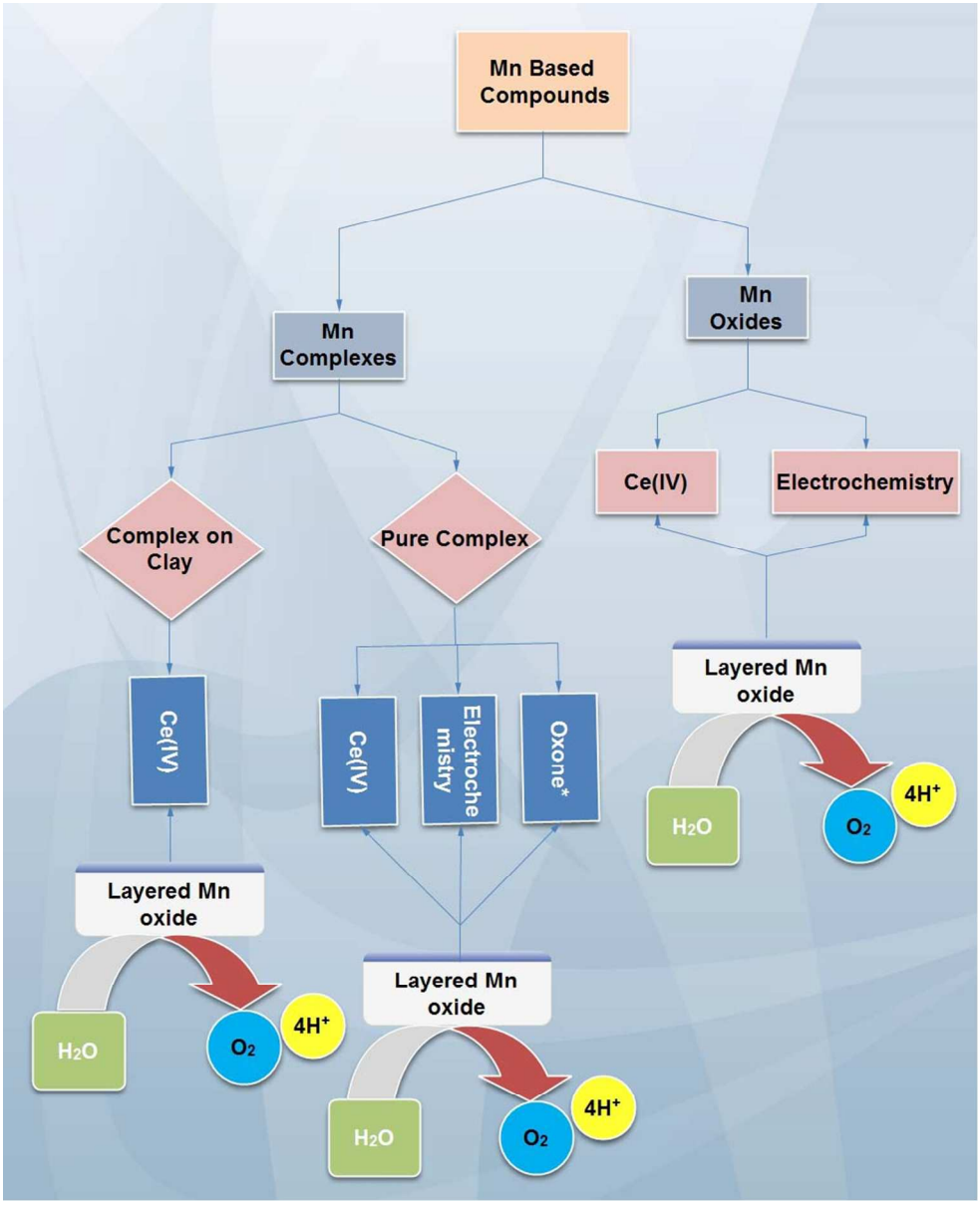


279x342mm (96 x 96 DPI)

Mn oxides may be true catalyst in the water-oxidation reactions of Mn complexes and oxidants.

Cite this: DOI: 10.1039/c0xx00000x

www.rsc.org/xxxxxx

ARTICLE TYPE

# The role of nano-sized manganese oxides in the oxygen-evolution reactions by manganese complexes: Towards a complete picture† ‖

**Mohammad Mahdi Najafpour,*[a,b] Małgorzata Hołyńska,[c] Amir Nasser Shamkhali,[d] Sayed Habib Kazemi,[a,b] Warwick Hillier,[e] Emad Amini,[a] Mostafa Ghaem Maghami,[a] Davood Jafarian Sedigh, ‡[a] Atefeh Nemati Moghaddam, ‡[a] Rahim Mohamadi, ‡[a] Sasan Zaynalpoor‡[a] and Katrin Beckmann‡[e]**

***Received (in XXX, XXX) Xth XXXXXXXXX 20XX, Accepted Xth XXXXXXXXX 20XX***
**DOI: 10.1039/b000000x**

Eighteen Mn complexes with N-donor and carboxylate ligands have been synthesized and characterized. Three Mn complexes among them are new and reported for the first time. The reactions of oxygen evolution in the presence of Oxone ($2KHSO_5 \cdot KHSO_4 \cdot K_2SO_4$) and cerium(IV) ammonium nitrate catalyzed by these complexes are studied and characterized by UV-visible spectroscopy, X-ray diffraction spectrometry, dynamic light scattering, Fourier transform infrared spectroscopy, electron paramagnetic resonance spectroscopy, transmission electron microscopy, scanning electron microscopy, membrane-inlet mass spectrometry and electrochemistry. Some of these complexes evolve oxygen in the presence of Oxone as a primary oxidant. $CO_2$ and $MnO_4^-$ are other products of these reactions. Based on spectroscopic studies, the true catalysts for oxygen evolution in these reactions are different. We proposed that for the oxygen evolution reactions in the presence of Oxone, the true catalysts are both high valent Mn complexes and Mn oxides, but for the reactions in the presence of cerium(IV) ammonium nitrate, the active catalyst is most probably a Mn oxide.

## Introduction

There has been considerable interest in the coordination chemistry of Mn complexes because of the significant involvement of Mn in various biological systems, including the oxygen-evolving complex (OEC) or water-oxidizing complex (WOC) in Photosystem II (PSII),[1-3] Mn peroxidase (MnP),[4] Mn thiosulfate oxidase,[5] Mn catalase,[6] ribonucleotide reductase,[7] acid phosphatase[8] and superoxide dismutase (MnSOD).[9] Mn complexes with N-donor and carboxylate ligands are of interest because these ligands are related to histidine, aspartate or glutamate residues that are present in the active site of these Mn-containing enzymes.

Water-oxidation reaction is one of the most important reactions not only because of its importance in PSII but also in energy conversion systems.[10] Water electrolysis for hydrogen production has been considered regarding the rising costs of fossil fuels and the growing environmental pollution. An efficient and stable water-oxidizing catalyst is of paramount importance for hydrogen production *via* water splitting.[10] Many metal ions were reported as efficient catalysts for water oxidation.[11] However, the use of these metals for global scale water oxidation is problematic owing to concerns about their low abundance in the earth's crust, toxicity, and high cost. Nature, utilizing very clever strategies, uses Mn as an abundant transition metal for water oxidation.[1-3] The OEC in PSII consists of a Mn-Ca cluster hosted in the environment of many amino acid chains (Fig. 1).[1-3]

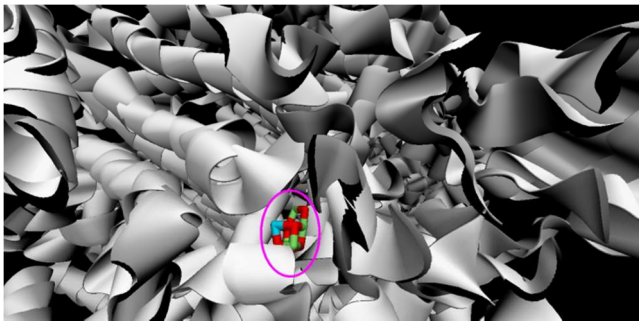

a

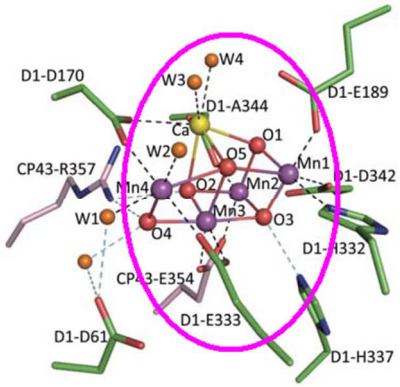

b

Fig. 1 $[Mn_4CaO_5(H_2O)_4]$ cluster (circled in magenta) and the surrounding amino acids in PSII (a). There is only a small fraction of N-donor and carboxylate groups that come in direct contact with the Mn-Ca cluster (the image was modified from ref. 2) (b).

Research on Mn complexes with carboxylate and N-donor ligands has also been the subject of numerous reports because of their interesting structural and redox properties.[12] It was reported that a few Mn compounds show oxygen evolution activity in the presence of Oxone or Ce(IV).[12] Among many Mn compounds, there is only one homogeneous Mn complex that may be a true and efficient water-oxidizing catalyst. This is the dinuclear Mn complex reported by Karlsson *et al.* that contains imidazole groups. The catalytic activity of the complex was investigated by addition of a 480-fold excess of the single-electron oxidant $[Ru(bpy)_3](PF_6)_3$ in phosphate buffer (pH 7.2).[13] $[(OH_2)(terpy)Mn(\mu\text{-}O)_2Mn(terpy)(OH_2)]^{3+}$ (terpy = 2,2';6',2"-terpyridine) and many Mn complexes with carboxylate and N-donor ligands were also reported as oxygen-evolving catalysts in the presence of Oxone.[12,14]

Turnover numbers (TON) of oxygen evolution for many of these complexes were less than 1.0 (mol oxygen per mol of catalyst). However, Mn oxides have been reported as good heterogonous catalysts for water oxidation.[15]

In this paper, we synthesized eighteen Mn complexes with carboxylate and N-donor ligands related to the amino acid-chains around Mn-Ca cluster (Fig. 1b). These complexes are characterized by elemental analysis, Fourier transform infrared spectroscopy (FTIR), electronic absorption spectroscopy (UV-Vis), electrochemistry, electron paramagnetic resonance (EPR). The reactions of these complexes with Oxone and Ce(IV) are also studied. Some of these complexes show oxygen evolution activity in the presence of Oxone with a TON of 0.1-0.5. Recently, Density Functional Theory (DFT) is reported as a powerful method to study the structural properties and electronic structure of transition metal complexes due to its reliable results in comparison with experimental data. This advantage of DFT is accompanied with its lower computational cost than post-Hartree-Fock methods.[16] Therefore, DFT calculations have been used for many investigations on the water-oxidizing Mn complexes, especially the oxygen-evolving center of PSII.[17-32] We also considered DFT calculations for deeper investigation of the structure of one of our complexes and its oxidized form.

## Experimental

### Materials and instrumentation

All reagents and materials used for the syntheses were reagent-grade and used without further purification. Solvothermal experiments were performed using a home-made Teflon and holder. Elemental analyses were performed on a Perkin-Elmer 2400 CHNS/O elemental analyzer. MIR spectra of KBr pellets of compounds were recorded on a Bruker vector 22 in the range between 400 and 4000 $cm^{-1}$. EPR Spectra were collected at 4 K for the samples in form of frozen solutions with an X-band Varian E-9 spectrometer equipped with an Oxford ESR-900 liquid helium cryostat. Typical instrument settings were the following: modulation amplitude 20 G, modulation frequency 100 kHz, and microwave power 2.0 mW. All electrochemical tests were performed in a conventional three- electrode cell with an Ag/AgCl (saturated) and platinum wire as reference and counter electrodes, respectively. Carbon paste electrode was employed as the working electrode and constructed by mixing the appropriate Mn complex (**16** and **17**) with Dioctyl phtalate (DOP, from Aldrich Company) and active graphite (in a ratio of 10:45:45). Electrical connection of the carbon paste electrode was established *via* a copper wire. Also, electrochemical studies of **15** were carried out in an acetonitrile solution containing 0.1 M of $LiClO_4$ as supporting electrolyte using a 0.0314 $cm^2$ glassy carbon electrode (as working electrode). All electrochemical measurements were done by using Autolab 101 (Autolab Eco Chemie B.V. Netherland).

All solutions were prepared using doubly deionized water. Oxone was standardized by iodometric titration and found to contain 0.21 mmol $KHSO_5$ per 100 mg. The acetate buffer was prepared by adjusting the pH of a 0.1 M KOAc solution to 4.5 with concentrated $H_2SO_4$. In a typical experiment, after the deaeration with nitrogen, a 0.015 M solution of a metal complex in water was added to a buffered solution of Oxone (100 ml, 0.021 M in 0.1 M acetate buffer, pH 4.5). All rates were measured at 25.0 °C using the method of initial rates from $t = 0$ to $t = 2$ min. Oxygen evolution from aqueous solutions in the presence of Ce(IV) was measured using luminescent DO probe type oxygen electrode (HQ40d portable dissolved oxygen meter) connected to an oxygen monitor with a digital readout. The sample chamber temperature was maintained at 25.0 $^oC$ with a circulating water bath. In a typical run, the instrument readout was calibrated against air-saturated distilled water stirred in the air-tight sample chamber under DO probe type oxygen electrode. After ensuring a constant baseline reading, the water was removed, and 40 ml of Ce(IV) solution was introduced into the sample chamber. After allowing time for equilibration (~1 min), Mn complex was injected into Ce(IV) solution. In control experiments, 1 ml of the blank solvent was added to 40 ml of the Ce(IV). The control readings were substracted from the sample readings to get the final oxygen-evolution data. The substraction of controls typically produced less than a 1% change in the oxygen-evolution data. The experimental setup consisted of a self-made jacketed glass cell with a threaded neck and a capillary side-arm for catalyst injection. The cell was charged with a Ce(IV) salt. The Ce(IV) salt (2.5 g) was dissolved in 40 ml water magnetically stirred at 25.0 $^oC$. Ce(IV) was stable under these conditions and oxygen evolution was not observed. After deaeration of the Ce(IV) salt solution with argon, the investigated complexes were added and oxygen evolution was recorded with the oxygen meter under stirring.

### X-ray diffraction

X-ray diffraction data for single-crystals of **15, 17** and **18** were collected on a STOE IPDSII diffractometer, employing graphite-monochromated $MoK_\alpha$ radiation (see Table S1 for basic X-ray data). All structures were solved by direct methods in SHELXS and refined in SHELXL software.[33] C-bonded H atoms were

generated in their calculated positions and a riding model was applied with $U_{eq}$=1.2/1.5$U_{eq}$ (parent atom) for aromatic/methyl H atoms, respectively. Water H atoms were found on difference Fourier maps and initially refined with restraints of 0.820(2) Å on the O-H bond lengths. Subsequently their parameters were constrained.

**15**: On the final difference Fourier map the highest peak of 0.28 e/Å$^3$ is located in the middle of the Mn1-O1 bond, 1.12 Å from O1 atom and 1.21 Å from Mn1 atom.

**17**: On the final difference Fourier map, the highest peak of 0.24 e/Å$^3$ is located in the middle of the Mn2-N122 bond, 0.81 Å from N122 atom and 1.50 Å from Mn2 atom.

**18**: N-bonded H atom was found on difference Fourier map and initially refined with restraint of 0.860(2) Å on the N-H bond length. On the final difference Fourier map the highest peak of 0.39 e/Å$^3$ is located 1.06 Å from Mn1 atom.

The crystal structures of **1**-**14**, **16** have been reported in literature. (For daials of structures see Table S1-S3 (ESI†)).

**Preparation of the Mn(II) complexes**

Cmplexes 1,[34] 2,[35] 3,[36] 4,[37] 5,[38] 9,[39] 10,[40] 11,[41] 12,[41] 13,[40] 14[43] and 16[44] were synthesized by previously reported methods (for detail see ESI†).

**Complex 15** (Mn(qterpy)$(CH_3COO)_2(H_2O)_2$, quaterpy: quaterpyridine: A mixture of $Mn(CH_3OO)_2{\cdot}4H_2O$ (0.2 g) and quaterpyridine (0.1 g) in methanol (30 mL) was heated at 50°C for 30 min., then the mixture was filtered. After filtration and slow evaporation in air for two weeks, pale-yellow crystals of complex **15** were formed.

**Complex 17** ($Mn(Phen)_2$(Naphthalene-1,8-dicarboxylato)$(H_2O)_2$): $MnCl_2$ : Phen : Naphthalene-1,8-dicarboxylic : NaOH (molar ratio: 1:2:1:2) and water (40.0 mL) were heated at 120 °C under hydrothermal conditions for 24 h. After filtration and slow evaporation in air for two weeks, yellow crystals were formed.

**Complex 18** (Mn(pyrazole-3,5-dicarboxylate)$(H_2O)_4$): $MnCl_2$:Pyrazole-3,5 dicarboxylate:NaOH (molar ratio: 1:1:2) and water (40.0 mL) were heated at 120 °C under hydrothermal conditions for 24 h. After filtration and slow evaporation in air for two weeks, yellow crystals were formed.

## Calculation Method

The structure of **17** and the oxidized form of this complex were optimized by B3LYP hybrid functional in which Hartree-Fock exact exchange is combined with Generalized Gradient Approximation (GGA).[30] For all of the calculations, LANL2DZ basis set with effective core potentials (ECPs) is used in order to reduce the computational cost of the calculations.[31,32] Using ECPs usually does not reduce the accuracy of DFT calculations due to the fact that DFT methods are not considerably sensitive to the basis set size.[45] All of the calculations are performed using Firefly quantum chemistry package,[46] which is partially based on GAMESS (US) source code.[47] The detailed results of the structures optimizations for both of the mentioned complexes are given in Table S4 of the Supporting Information. Also Mulliken charges and pure spin values [α(↑)-β(↓)] of the selected atoms in complex **17** and its oxidized states are given in Tables S4, S5 and S6 (ESI†), respectively.

## Results and discussion

### X-ray diffraction data

We used pure crystalline form of each complex in our experiments. Identity of all crystalline compounds was confirmed by the corresponding cell constants measurements. However, **15**, **17** and **18** are compounds with crystal structures reported for the first time. Structures of some complexes are shown in Scheme S1 (ESI†).

### Structure of 15

**15** is monohydrate of a mononuclear Mn(II) complex in which the central Mn(II) ion is chelated by a tetradentate 2,2':6',2'':6'',2'''-quaterpyridine (QP) ligand (Fig. 2, Fig. S1 and S2 (ESI†)).

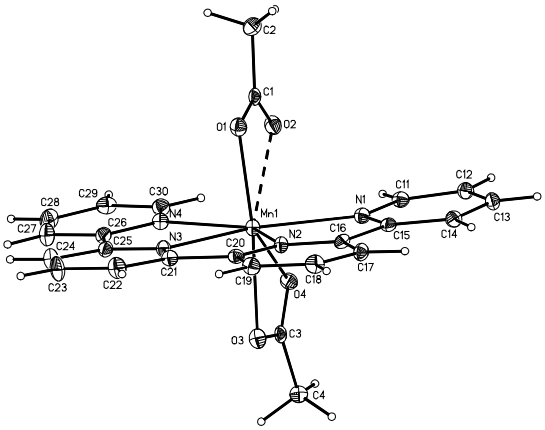


Fig. 2 Molecular structure of **15** with thermal ellipsoids plotted at 30% probability level. The semi-coordination Mn1-O2 bond (see Text) is denoted with dashed line.

The apical positions in the Mn(II) ion coordination sphere in **15** are occupied by bidentate acetate ions. The known crystal structures[48] of mononuclear transition metal QP complexes include transition metal mononuclear complexes (Cu[49,50] Co[50,51], Mn,[51] Pd,[52] Re,[53] Fe,[54] Pt,[55] Ag,[56] Zn,[57] Ni,[57,58] Y,[59] W,[60] $[Ag_2]$,[58] oxo-bridged $[Fe_2]$ ,[61] heterometallic Ni-V[62] as well as main group Pb(II) complexes.[63] In the majority of these complexes the QP ligand adopts its usual tetradentate coordination mode, also observed in **15**. In **15** three Mn-O(acetate) bonds are in the 2.247(2)-2.344(2) Å range (Table S2). The Mn1-O2 bond of 2.606(2) Å length may be considered as a secondary coordination bond, even shorter than e.g. the 2.850(3) Å value reported by Cady *et al.* for their six-coordinate Mn(II) complex serving as a model for associative substitution.[64]

Chin-Wing Chan *et al.*[51] reported on similar cationic complexes, $[Mn(QP)(H_2O)(OAc)]^+$ and $[Mn(QP)(H_2O)_2]^{2+}$ isolated as perchlorate salts. The $[Mn(QP)(H_2O)(OAc)]^+$ complex differs

with respect to **15** by substitution of one acetate ligand with water ligand. The void angle of the chelating QP ligand in **15**, N1-Mn1-N4, of 151.82(6)°, is similar to the analogous values given by Chin-Wen Chan *et al.*[51] **15** is isolated as a monohydrate. The water molecules of hydration participate in formation of hydrogen bonds to create hydrogen-bonded layers (Fig. S1, Table S3) parallel to (011) (Fig. S2). This complex is unstable in water, where decoordination of the organic ligand takes place.

**Structure of 17**

**17** is a mononuclear Mn(II) complex with two bidentate N-donor phenanthroline ligands, one monodentate naphthalene-1,8-dicarboxylate ligand and one water ligand in the Mn(II) ion coordination sphere, isolated as a hydrate (Fig. 3, Fig. S3). The water ligand is donor to an intramolecular hydrogen bond with the free carboxylate O atom of the naphthalene-1,8-dicarboxylate ligand acting as acceptor (Fig. 3, Table S3; Fig. S3-S5 (ESI†)).

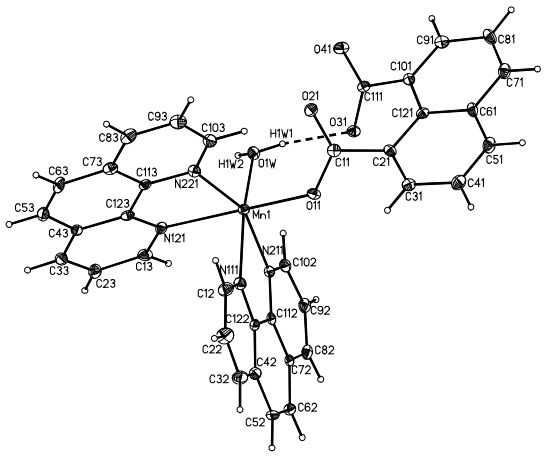


Fig. 3 Molecular structure of **17** on the example of one of the symmetry-independent molecules**.** Thermal ellipsoids are plotted at 30% probability level. H atoms are shown as spheres of arbitrary radii. Intramolecular hydrogen bonding is shown with dashed lines.

Naphthalene-1,8-dicarboxylate ligand has been used for the construction of coordination polymers.[65]

There are two symmetry-independent complex molecules in **17** (**A** and **B**, respectively, Fig. S3a-b) and eight water molecules of solvation. The two molecules slightly differ in interplanar angles between the planes of aromatic ligands, especially with respect to one phenanthroline (phen) ligand and the carboxylate ligand naphthalene ring: phen-N111(N122)/phen-N121(N112): 75.5(1)/77.0(1)°; phen-N111(N122)-naphthalene ring: 88.7(1)/86.2(1)°; phen-N121(N112)-naphthalene ring: 78.6(1)/83.6(1)° (see Fig. S3c for the relevant overlap diagram). In the naphthalene-1,8-dicarboxylate ligand planes of the carboxylate groups are twisted with respect to the naphthalene ring plane: for the carboxylate group coordinated to the Mn(II) ion the relevant interplanar angle is 46.4(2)/43.6(2), for the non-coordinated group: 45.2(2)/47.4(1)° for **A**/**B**, respectively. Each Mn(II) ion coordination sphere is distorted octahedral with Mn-N bond lengths at 2.263(2)-2.317(2) Å range, Mn-$O_{carboxylate}$ bonds of 2.095(2)-2.108(2) and Mn-$O_{water}$ bonds of 2.130(2)-2.133(2) Å length. As expected, on participation in the Mn(II) coordination sphere the C-O(carboxylate) bond length increases (Table S2, O31-C111, O12-C14 bonds).

Water molecule in **17** participates in hydrogen bonding to create extended cluster-like motifs (Fig. S4a-b, Table S3) linked into chains extending along [011] (Fig. S5).

Compound **17** may be regarded as a model for proton-coupled electron transfer as the proton may be easily transferred between water and carboxylate ligand accompanied by an electron transfer:

Mn(II)-OH···O(carboxylate) → $e^-$ + Mn(III)-O···HO(carboxylate)

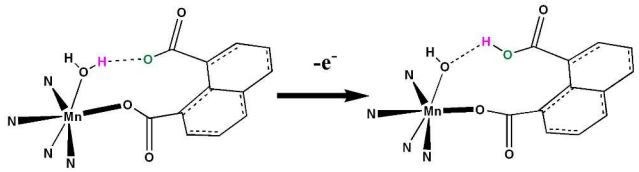


Scheme 1 This structure may be regarded as a model for the proton-coupled electron transfer as the proton may easily transferred between water and carboxylate ligand, accompanied by an electron transfer.

To design such complexes the $pK_a$ (acidic constant) for the base group (carboxylate group in compound **17**) should be between $pK_a$ for M(II)-$OH_2$ and M(III)-$OH_2$. Deprotonation prevents from charge accumulation on the metal ion. We also studied **17** and its oxidized form by DFT calculations. The most important result of the DFT calculations is confirmation of the existence of a hydrogen bond between O31 and H1W1 in complex **17** in which O31-H1W1 and O1W-H1W1 bond lengths are 1.1561 Å and 1.2587 Å, respectively as given in Table S4. When Mn(II) in **17** is oxidized to Mn(III), these distances are 1.0041 Å and 1.7362 Å, respectively. Therefore, H1W1 atom is completely removed from O1W and attached to carboxylate in the form of oxidized complex. The results of Barry and co-workers on the OEC in PSII showed that oxidation of Mn, during the $S_1$ to $S_2$ transition, strengthens hydrogen bonding to peptide carbonyl groups.[66]

**Structure 18**

**18** is hydrate of a mononuclear Mn(II) complex including bidentate N,O-coordinated 3,5-pyrazoledicarboxylate ligand and four water ligands in the central ion coordination sphere (Fig. 4; Fig. S6-S8 (ESI†)).

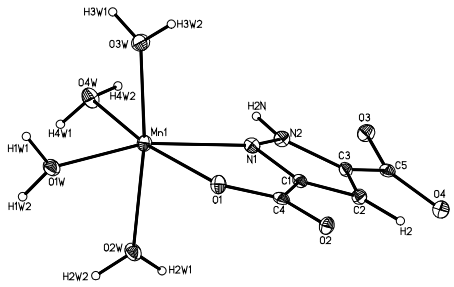

Fig. 4 Molecular structure of **18** with atom labeling scheme. H atoms are shown as spheres of arbitrary radii. Thermal ellipsoids are plotted at 30% probability level.

Both carboxylic groups of the 3,5-pyrazoledicarboxylate ligand are deprotonated, whereas one of the N sites remains protonated (see Experimental). An analogous Ni(II) complex was introduced by King *et al.*[67] displaying an analogous coordination mode with one protonated pyrazole N atom and both deprotonated carboxylate groups, only one of which participates in the central metal ion coordination sphere. Known Mn(II) complexes of the 3,5-pyrazoledicarboxylate ligand are dimeric[68,69] or polymeric.[70,71] One of the two independent water molecules of solvation in **18** lies in special position on a two-fold symmetry axis. The central Mn(II) ion coordination sphere is distorted octahedral with Mn-$O_{water}$ bonds at 2.119(2)-2.212(2) Å range, Mn-$O_{carboxylate}$ bond of 2.217(2) Å length and Mn-$N_{pyrazolate}$ bond of 2.265(2) Å length.

In **18** a three-dimensional hydrogen-bonded network is formed with water molecules acting as donors/acceptors to O-H…O hydrogen bonds involving also carboxylate O atoms from the complex molecules as acceptors (Figs S7-S8, Table S3). The second kind of hydrogen bonding in **18** are N-H…O hydrogen bonds with pyrazole N atoms as donors and symmetry-related carboxylate O atoms as acceptors (Table S3). Figures S7-S8 show two different views of the crystal structure. Detals for structures (15, 17 and 18 are in Table S1-S3 (ESI†)).

**IR spectra**

In IR spectra of these compounds, bands at 3200-3550/1600-1630 $cm^{-1}$ corresponding to lattice water are related to antisymmetric and symmetric OH stretching/HOH bending modes, respectively.[72-75] Detection of the O-D bending vibrations of $D_2O$ molecules during the S-state cycle of the oxygen evolving complex in PSII has been reported. The characteristics of the weakly D-bonded OD stretching bands were consistent with the insertion of a substrate from the internal water molecules in the $S_2 \rightarrow S_3$ and $S_3 \rightarrow S_0$ transitions.[76] It was reported that FTIR detection of the DOD bending vibrations is a powerful method for investigating the molecular mechanism of photosynthetic water oxidation, as well as other enzymatic reactions involving functional water molecules. The reactions of water molecules were detected by monitoring the OH and OD stretching vibrations in the regions of 3800-3000 and 2200-2800 $cm^{-1}$,[76] respectively.

As a molecular model for the Mn cluster in PSII, IR spectrum of **9** displays a medium and broad absorption bands at about 3400 $cm^{-1}$, for the stretching vibrations of $H_2O$ (Fig. S9, ESI†). The sample of **9** was also moderately deuterated in 95% $D_2O$. The IR spectrum of the deuterated complex displays a medium absorption band at 2536 $cm^{-1}$, assignable to the stretching vibrations of $D_2O$. Two absorption bands are also observed at 2316 and 2513 $cm^{-1}$ (Fig. S9, ESI†). Only uncoordinated water molecules are present in the structure of **9**, so the peaks are related to uncoordinated water molecules around Mn. These results can be important to detection of the bulk water around Mn ions in PSII.

Very strong and sharp absorption bands at about 1680 and 1447 $cm^{-1}$ in **1**, **2** and **9-12** can be assigned to the antisymmetric stretching vibrations and symmetric stretching vibrations of the carboxylate groups. The value of $\Delta\upsilon_{as-s}$ ($\upsilon_{as}$(COO)-$\upsilon_{s}$(COO)) is larger than 200 $cm^{-1}$ indicating a monodentate coordination mode of the carboxylate groups.[72,73] The peaks revealing the presence of phen or bpy in **3-9** are present in the ranges 3100-2900 $cm^{-1}$ (aromatic C-H stretching vibrations), 1600-1550 $cm^{-1}$ ($\nu$ (C=N) and $\nu$ (C=C) stretches), 1470-1020 $cm^{-1}$ ($\nu$(C=C) + $\nu$ (C=N) vibrations), and 810-710 $cm^{-1}$ (aromatic C-H deformation vibrations).[74,75]

**Electronic spectra**

The electronic spectrum recorded for **1** shows very strong absorption bands at 200 nm and 264 nm, attributed to n-π and/or π-π* charger transfer within the ligand itself.[77, 78] The shoulder of the band at 400 nm can be attributed to d-d transitions.[79] The electronic spectrum of **1** can be compared to those of several mononuclear Mn(III) complexes, which exhibit d-d bands in this region.[79] The electronic spectra of **2** and **9-12** show only very strong absorption bands at ~225 nm and 264 nm, which are attributed to n-π and/or π–π* charger transfer within the ligand. The electronic spectra of **3-8** show very intense multiple absorption bands in the high energy region (~200, 220 and 260 nm) corresponding to n-π and/or π–π* charge transfer of the ligands.[80] Other complexes show a similar pattern in their electronic spectra.

**EPR Spectra**

The broad EPR signals above and below g = 2 due to the S = 5/2 zero-field splitting have been reported for other distorted mononuclear Mn(II) complexes.[81-86] Similar spectra for all Mn(II) compounds reported here are observed in 4 K. In the reaction of **1-10** and Oxone, an Mn(III/IV) dimer is formed and detected by EPR. Formation of similar Mn(III/IV) dimers was observed in the reactions of many Mn complexes (with N-donor and carboxylate ligands) with Oxone (Fig. S10, ESI†).[87]

It is assumed that the structure of the investigated species observed in the solid-state is preserved in solution, which is likely to hold for most solvents with low polarity and limited coordination abilities. But for polar solvents able to promote ligand exchange (water or DMSO), significant structural modifications may occur, which would drastically change the structure of the solvated complex, while promoting equilibria with other species stabilized by solvation.[88-91] In a simple solution of Mn(II) or Mn(III), many different species containing Mn may be formed because of the lability of Mn(II) and Mn(III).[91] So adding oxidants to these solutions yields many different high-valent Mn complexes depending on the reaction conditions.[88-91]

**Oxygen evolution in the presence of Oxone**

All reported reactions in this paper were carried out in buffered aqueous solutions over the pH = 4.5 using 0.021 M Oxone, as the Oxone salt is stable to decomposition in this pH.[87] No signs of $O_2$ evolution were observed with $MnSO_4$, $MnCl_2$, $Mn(CH_3COO)_2$,

$KMnO_4$, **6-8**, **11** and **12** as starting materials under these conditions. **1-5**, **9-10** are able to catalyse $O_2$ evolution. The range of 0.1-0.5 for TON parameters (mol $O_2$/mol Mn complex) was observed when these complexes were added to Oxone (0.021 M, pH= 4.5) (Table 1).

Table 1. The experimental rate laws and TON of $O_2$ evolution for **1-10** (C = Concentration of complex).

For bidentate ligands, the increase in TON with increasing of the ratio of the ligand(s) to metal (**1**>**2** and **3**>**4**>**5**) was observed. In the case of **3-5**, the TON parameter for oxygen evolution is related to the amount of the ligand which shows that the ligand is important in oxygen evolution at least in one pathway. Limburg *et al.* reported an $O_2$-evolving reaction between $[Mn(dipic)_2]^-$ (dipic = pyridine-2,6-dicarboxylate) and potassium peroxomonosulfate (Oxone).[92] **9** is an Mn(II) complex with pyridine-2,6-dicarboxylate. In **9**, Mn is hexacoordinated in a distorted octahedral geometry, chelated by four O atoms and two N atoms from two pyridine-2,6-dicarboxylate ligands.[39] The TON parameter of 0.3 was observed when a solution of **9** was added to Oxone (0.021 M, pH= 4.5). Another product in these oxygen evolution experiments for **1**, **2** and **9-12** is $MnO_4^-$ (Fig. S11, ESI†).

It would be expected[87] that in these complexes, the more carboxylate groups are present, the easier it would be to form $MnO_4^-$ and this is also observed.

A slower rate of dissociation of the ligand and slower formation of the $MnO_4^-$ ions are observed for N-donor ligands. Thus, it is not surprising that N-donor ligands are better for design of oxygen-evolving Mn-based catalysts. These results are consistent with the results obtained by other groups.[87] We found that the product of the reduction of Mn complexes with N-donor ligands is Mn oxide, rather than $MnO_4^-$. The transient absorptions derived from mixing Oxone and **1-12** show the distinctive UV–Vis absorbances between 400 and 500 nm, consistent with the presence of high-valent Mn species (Fig. S11, ESI†).[87]

An important issue regarding the oxygen evolution experiment by Mn complexes are the results obtained by membrane-inlet mass spectrometry (MIMS)[93-95] in $H_2{}^{18}O$. It is interesting to note, that different complexes show a different ratio of $^{32}O_2$,$^{34}O_2$ and $^{36}O_2$:[95]

Table 2 Isotope fractions of the evolved oxygen (in %) for the reactions of the complexes a–f[95] and **16.** Structures of the complexes a-f are shown in Scheme S2 (ESI†).

| Complex | $H_2{}^{18}O$ added (%) | $^{32}O_2$ | $^{34}O_2$ | $^{36}O_2$ |
|---|---|---|---|---|
| **a** | **10** | **80.8** | **18.1** | **1.0** |
| **b** | **10** | **89.2** | **10.4** | **0.4** |
| **c** | **10** | **91.1** | **8.8** | **0.03** |
| **d** | **10** | **93.6** | **8.2** | **0.2** |
| **e** | **10** | **81.5** | **17.4** | **1.1** |
| **f** | **13.8** | **74.3** | **25.0** | **0.6** |
| **16** | **13.8** | **84.3** | **15.6** | **~ 0.1** |
| **Mn oxides** | **5** | **95.1** | **4.9** | **~ 0** |
| **Theoretical** | **10** | **81.0** | **18.0** | **1.0** |
| **Theoretical** | **13.8** | **74.3** | **23.8** | **2.0** |

From Table 2 and Fig. 5, we conclude that there are two mechanisms for oxygen evolution catalysed by the complex. One is similar to the mechanism previously reported by the Brudvig's group[96a] with a high valent Mn complex as an intermediate that clearly led to the evolution of $^{36}O_2$ as a product, and another proposed catalyst is Mn oxide as we will discuss in next sections. When we analyzed the isotope fractions of the oxygen evolved by the Mn complexes, the fraction of $^{36}O_2$ turned out to be lower than the number predicted in many cases, and the fraction of $^{36}O_2$ was ~ 0 for Mn oxides. We related the lower numbers to the role of Mn oxide in oxygen evolution that produced no $^{36}O_2$ and lower content of $^{34}O_2$ than predicted by theoretical calculations. Mn oxide formation under these conditions is not surprising as Oxone is a very powerful oxidant (1.82 V vs. NHE). Based on the hypothesis assuming Mn oxide formation, we expect a low fraction of $^{36}O_2$ for unstable complexes. To test this hypothesis, we measured the fraction of $^{36}O_2$ for **16** as an unstable complex in the presence of Oxone. Results, as expected based on the hypothesis, display that in the first run for **16** the MIMS shows low $^{36}O_2$ content connected with the formation of an $Mn_2{}^{III,IV}$ complex that decomposes immediately after some oxygen evolution. It is interesting to note that in the second run the complex is, most probably, decomposed to Mn oxide and no $^{36}O_2$ formation was observed.

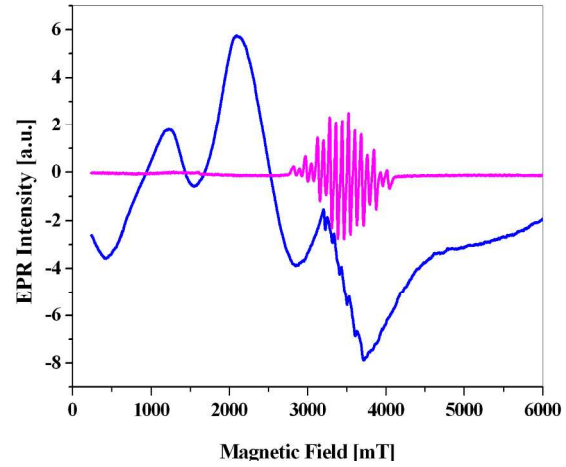


a

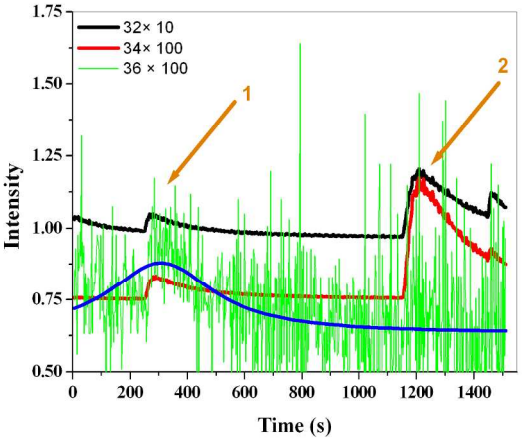

b

Fig. 5 EPR spectrum of **16** (blue). EPR spectrum of the mixture obtained in reaction between **16** (1 mM) and Oxone (0.023 M), frozen within 10 s of mixing. This 16-line spectrum is characteristic of di-μ-oxo bridged mixed-valence Mn (III/IV) complexes (pink) (a).[96b] The experimental fraction of oxygen evolution by **16** in the presence of Oxone under the conditions reported in Table 2. FFT Filter Smoothing of the experimental fraction of $^{36}O_2$ of **16** (blue) (b). The orange arrows show run 1 and 2.

Ligand oxidation may be important for all complexes under these conditions. For example heterocyclic N-oxides were detected[91] as products in the reactions of Oxone with **6-8**. A few minutes after the reaction between these complexes with Oxone, formation of brown colloidal particles is observed, detectable by SEM, TEM and DLS (Fig. 6). TEM images show that the small particles (~10 nm) are formed in the reaction of Mn complexes and Oxone. DLS shows that the particles grow bigger in the time scale of the experiment. The IR spectra recorded for these brown colloidal particles show low amounts of organic groups, which suggests formation of Mn oxides. Thus, the products of the reaction of Mn complexes with Oxone should be Mn oxides, the Mn(III/IV) dimer and $MnO_4^-$.

The reaction of Oxone with these reported complexes here produces a brown solid with few organic groups and strong peaks for Mn-O bonds as evidenced by IR spectra (Fig. S12, ESI†).

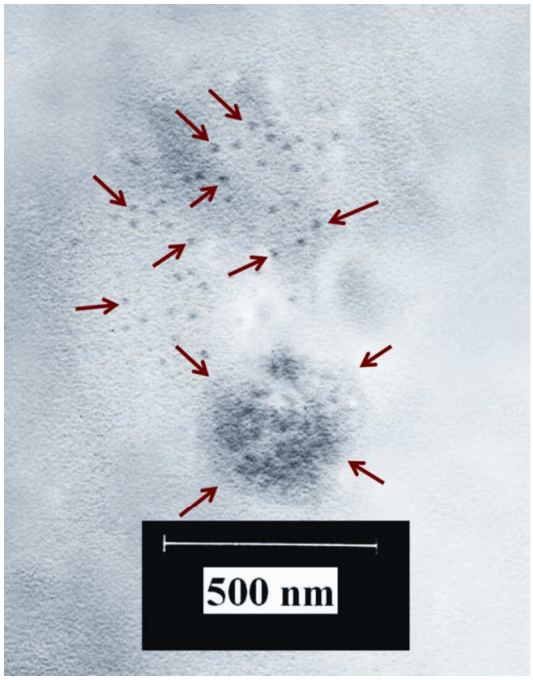


a

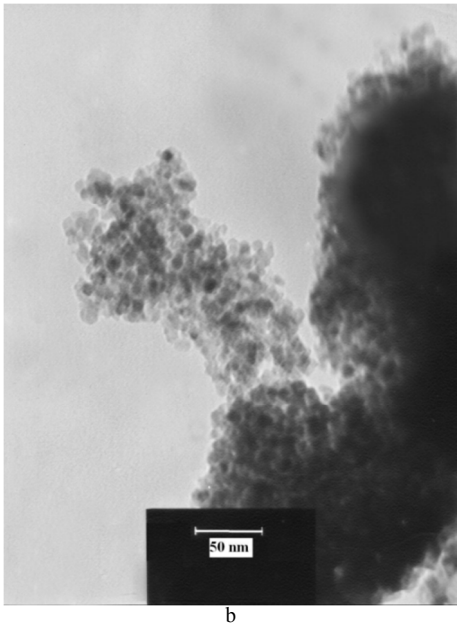


b

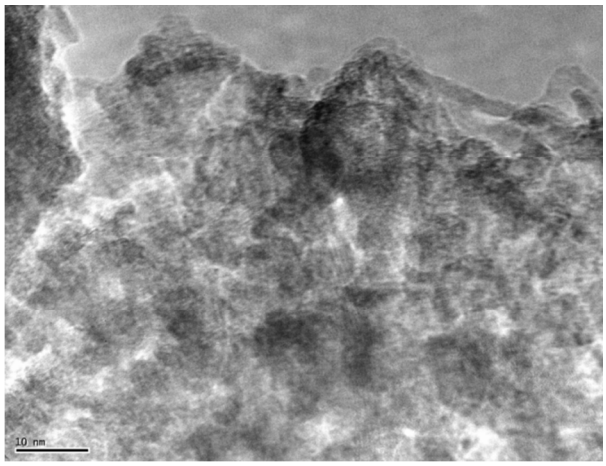


c

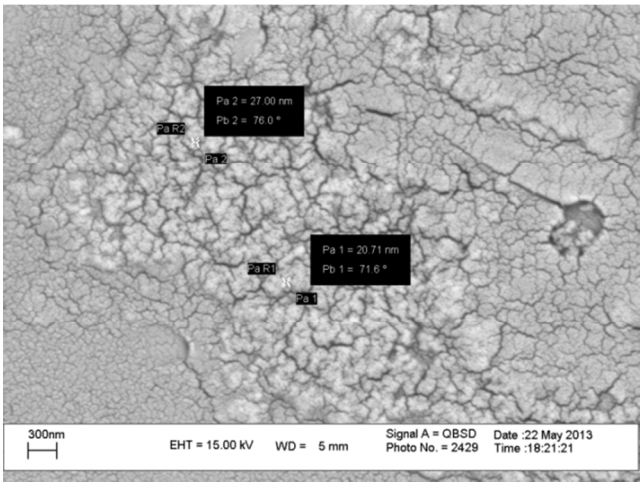


d

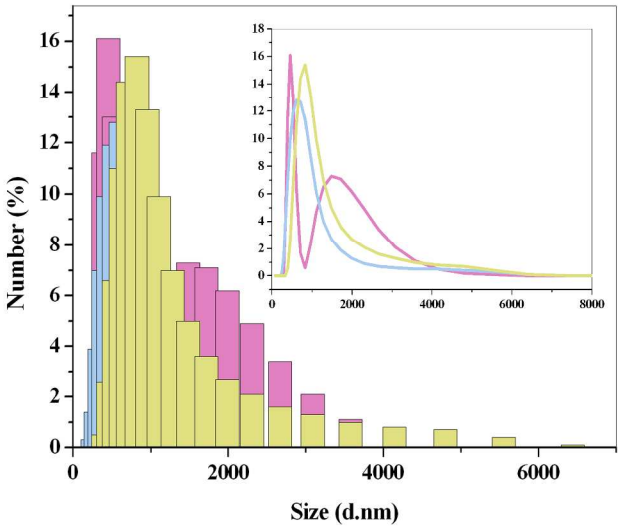


Fig. 6 TEM (a-c) and SEM (d) images of the resulting solution from the reaction of **16** with Oxone (0.023 M). Contrast for c is 55% and the arrows show some nanoparticles. Scale bar in (c) is 10 nm. Size distribution of the particles after 5 (blue), 10 (yellow) and 20 (magenta) minutes the reaction of **16** with Oxone (0.023 M) (e).

It is important to note that some research groups reported decoordination of multi N-donor ligands[51] (for example **15**) in the reactions with water molecules and $[Mn(H_2O)_6]^{2+}$ formation in water, which can be explained based on the hard-soft acid and base theory. The reaction of peroxomonosulfate ion, $HSO_5^-$, with the $[Mn(H_2O)_6]^{2+}$ ions can lead to Mn oxides formation. In pH~ 4.5, the product is Mn(IV) oxide, whereas in 1.25 M $H_2SO_4$ peroxide decomposition is the major reaction with small amounts of Mn(III) being detectable.[98] Using the "competing acceptor" method, it was established that the sulfate radical anion is formed during the reaction.[98]

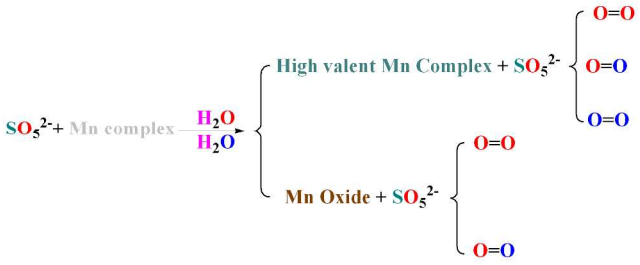


Scheme 3 Proposed intermediates in the reaction of Oxone and Mn complexes.

## Electrochemistry

Electrochemical oxidation of $[Mn^{II}(L)_3]^{2+}$ (L= bpy or phen) in acetonitrile is known to lead to the mixed-valent di-$\mu$-oxo bridged binuclear complexes $[Mn^{III,IV}(O)_2(L)_4]^{3+}$.[99-103] More oxidation of these mixed-valent complexes is followed by a second dimerization process to form additional oxo-bridges ($[Mn_4^{IV}O_6(L)_6]^{4+}$).[99-103] In acetonitrile, the oxidation of Mn(II) in the $[Mn^{II}(bpy)_3]^{2+}$ complex to Mn(III) has more positive potential than an analogous reaction of the corresponding phenanthroline complex. This trend is reversed for the redox reactions that involve the di-µ-oxo di-Mn groups. The shift in redox potentials does not follow a linear free energy relationship.[99] It is also reported that the shape of the cyclic voltammograms of **6** in the positive potential range depends on the potential scan rate used. At a low scan rate (20 mV $s^{-1}$), the electrochemical behaviour of **6** in acetonitrile is close to that observed in a buffered aqueous medium with a broad oxidation peak at 0.84 V (vs. Ag/0.01 M $AgNO_3$ reference electrode) (shoulder) corresponding to the $Mn^{II}/Mn^{III}$ redox couple.[99-103] This $Mn^{III}$ species reacts rapidly with residual water contained in the solvent *via* a disproportionation reaction to form the binuclear di-µ-oxo $[Mn_2^{III,IV}O_2(bpy)_4]^{3+}$complex.[99-103] The formation of $[Mn_2^{III,IV}O_2(bpy)_4]^{3+}$ ions is displayed by the presence of a reversible oxidation system at $E_{1/2}$ = 1.02 V (vs. Ag/ 0.01M $AgNO_3$ reference electrode) leading to the $[Mn_2^{III,IV}O_2(bpy)_4]^{4+}$ complex. In this paper, we study electrochemistry of the $[Mn^{II}(L)_n]^{2+}$ complex (n= 1, 2 or 3, L= bpy or phen) in water at pH = 4.5 (acetate buffer) under the same conditions, similar to the conditions applied in the experiment with Oxone used as an oxidant. The cyclic voltammograms of **3-5** with different scan rates exhibit an irreversible broad oxidation peak around 0.3 V, corresponding to the metal oxidation process Mn(II)/Mn(III) (Fig. 7).

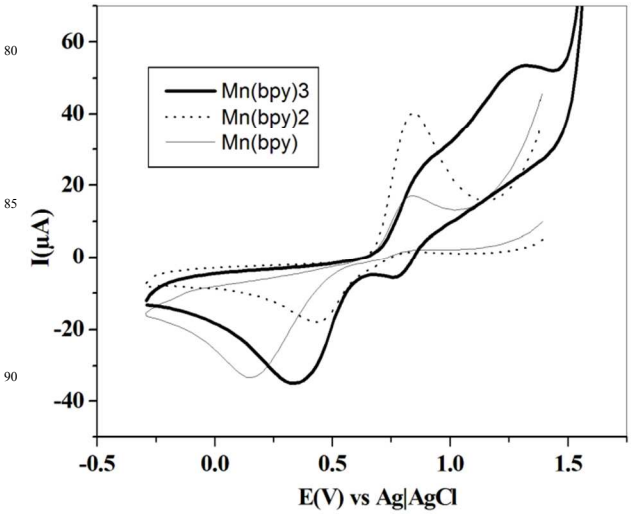


Fig. 7 Cyclic voltammograms in aqueous buffer at pH 4.5 (scan rate 100 mV $s^{-1}$) of a 2 mM solution of **6-8**.

**6-8** display similar cyclic voltammograms with an irreversible broad oxidation peak around 0.9 V. **6** has an additional irreversible broad oxidation peak around 1.27 V, related to multinuclear high-valent Mn complexes.[102] Under these conditions other complexes are not soluble enough (**1**, **9-10**) or they exhibit no oxidation peaks (**11-12**).

It is reported that by the addition of $Cl^-$, oxidation processes of Mn(III)(L)X (L= Salen or Salpn, X = $Br^-$) improve from quasi-reversible to reversible, and their oxidation products, $[Mn(IV)(L)X]^+$ are stabilized by the combination with $Cl^-$, resulting in $[Mn(IV)(L)Cl_2]$.[103] Effect of the $Cl^-$ ions presence (2.0 M) was tested in the electrochemical studies of **6-8**. The $Cl^-$ anions have no effect on the metal oxidation process

Mn(II)/Mn(III), but have a small effect on the irreversible broad oxidation peak around 1.27 V, related to multinuclear high-valent Mn complexes in **6** (Fig. S13, ESI†).

Fig. 8 presents the voltammetric behavior of **17** (cycle number 25) in an acetate buffer solution adjusted to pH = 5. As clearly seen, a broad oxidation peak is located between 800 to 1200 mV *vs.* Ag/AgCl electrode, which could be attributed to the Mn(II)/Mn(III) oxidation. As previously reported, after ligand decomposition, Mn(II) can be oxidized to Mn(III) and consequently in a disproportion reaction Mn(III) will convert to Mn(II) and Mn(IV).[104] Hence, in scanning to the positive potentials Mn(II) could produce $MnO_2$, which is a stable form of Mn in this condition.[105] By increasing the potential cycling, the peak current due to conversion of Mn(III) to Mn(IV) is increased. It might arise from the fact that the amount of the Mn oxide will increase after successive potential scans, due to continuous conversion of the Mn complex to $MnO_2$. In other words, many Mn complexes in water and at high potential decompose to Mn oxide.

Fig. 8b shows the successive voltammograms recorded for **16** in acetate buffer at pH = 5. As mentioned above for **17**, in the first cycle the Mn(II)/Mn(III) oxidation peak appeared. By successive potential cycling, the first irreversible process (Mn(II)/Mn(III) oxidation) is replaced by Mn(III)/Mn(IV) redox behavior. Additionally, the peak potential was shifted to the more positive potential and a reduction peak was observed. The electrochemical behavior of both **16** and **17** complexes is similar to the electrochemistry of the carbon paste electrode of Mn oxide. Thus, it could be concluded that both **16** and **17** complexes are not stable under potential cycling. From these electrochemical studies, we can conclude that many Mn complexes decompose before any water oxidation process can take place in such high potential.

**15** is not stable in water. Thus, we considered electrochemistry of the complex in acetonitrile. Fig. S10c (ESI†) presents the voltammetric behavior of **15** dissolved in acetonitrile solution containing 0.1 M of $LiClO_4$ as supporting electrolyte at a scan rate of 100 mV/s. As it is obvious, a pair of broad redox peaks appeared, indicative of quasireversible redox behavior of Mn. It should be mentioned that the free ligand (quaterpyridine) did not show significant redox behavior between +1 to -2 V *vs.* reference electrode. Hence, it could be concluded that the redox peaks originated from the oxidation-reduction Mn(II)/Mn(III).

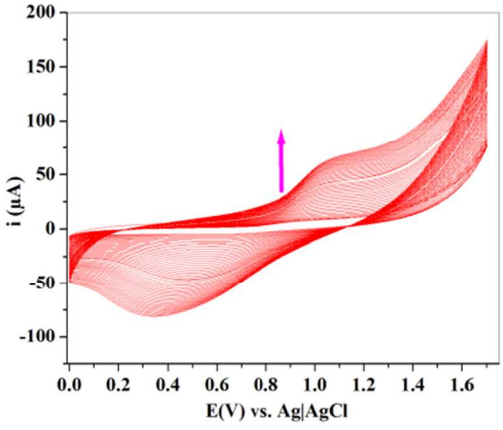


a

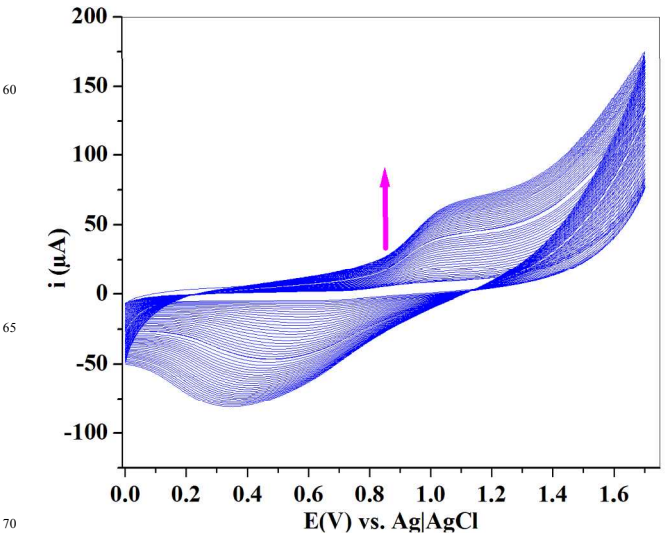


b

Fig. 8 Cyclic voltammograms (cycle numbers 2-50) recorded for the carbon paste electrode containing **17** at a scan rate of 100 mV/s in an acetate buffer solution with pH = 5 (a). Cyclic voltammograms (cycle numbers 2-50) recorded for the carbon paste electrode containing **16** at a scan rate of 100 mV/s in an acetate buffer solution of pH = 5 (b).

**Evidences from other groups: True catalysts in electrochemical water oxidation by Mn complexes**

The effect of the Mn precursors on $MnO_2$ formation in electrochemical experiments is considered by William H. Casey and Leone Spiccia's groups.[106a] $[Mn_4O_4L_6]^+$ (L: diarylphosphinate), embedded into a Nafion polymer matrix was reported as an efficient water-oxidizing electrocatalyst.[106b] Some methods probed the fate of the cluster within Nafion and provided some evidence supporting the presence of an intact cubane structure in Nafion. In 2011, William H. Casey and Leone Spiccia's groups showed a mechanism for water oxidation by the compound.[106a] They showed evidence that the cluster dissociates and forms a disordered Mn(III/IV) oxide phase. Recent data from Spiccia' group showed that many Mn complexes under similar conditions decompose to nanoparticulate $MnO_x$, formed in Nafion polymer.[106a] This nano-sized Mn oxide oxidizes water under neutral pH conditions with the onset of electrocatalysis occurring at an overpotential of only 150 mV. The group also found that the structure of the complexes is an important factor for the controlled formation of a nano-sized Mn oxide.[106c] These organic/Mn oxide compounds are promising catalysts for water oxidation.[106d]

**The reaction of Ce(IV) with solid Mn complexes or their solutions**

M. M. Najafpour and A. Nemati Moghaddam previously investigated the reaction of some of Mn complexes with Ce(IV).[107] Here, we found that all Mn complexes reported here (concentration $10^{-4}$-$10^{-5}$ M) in solution and in the presence of

Ce(IV) produced a brown solution, $MnO_4^-$, and $CO_2$. $CO_2$ could be detected in the reaction with a $BaCl_2$ solution. At low concentrations of Ce(IV) (2:1 Ce : complex), the EPR spectrum confirms the formation of Mn(III/IV) dimers in the reaction of **3-8** with Ce(IV), showing characteristic 16-line signals (Fig. 9). $[Mn_2O_2(bpy)_4][Ce(NO_3)_6]\cdot 5H_2O$ and multinuclear Mn complexes such as $[Mn_3O_4(phen)_4(H_2O)_2](NO_3)_4\cdot 2.5H_2O$ are synthesized and characterized by the Rajasekharan's group using Ce(IV) as oxidant.[108,109]

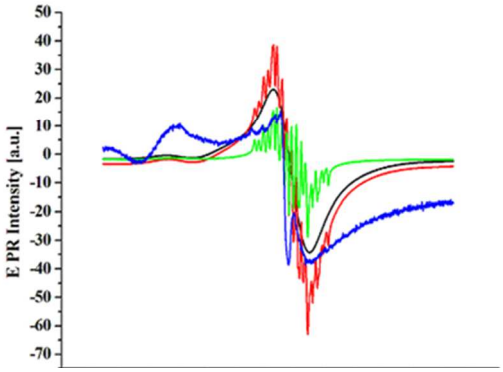


Fig. 9 EPR spectrum of **3** (black), the reaction mixture of **3** (0.1 mM) and Ce(IV) (1.0 mM) (blue), the reaction mixture of **3** (1 ml, 1 mM) and Oxone (0.25 mL, 0.023 M) (green) and the sum of green and black spectra (red).

Adding more Ce(IV) to these Mn(III/IV) dimers, as used in water oxidation reactions, produces Mn(III) complexes, a brown solution and $MnO_4^-$. At high concentrations of the Mn complex on addition to the brown solution, brown particles formation was also observed. Thus, Mn complexes should be considered as heterogonous catalysts for water oxidation under these conditions.

All Mn complexes studied here as heterogeneous or homogeneous catalysts decomposed to a brown solution compound displaying a UV-Vis band at $\lambda_{max}$ ~ 410 nm, very similar as in the spectrum of the previously reported $[Mn(H_2O)_6]^{3+}$ ion.[107] More interestingly, mixing of solutions of $Mn(NO_3)_2$ and Ce(IV) produced a brown solution with a UV-Vis band at $\lambda_{max}$ ~ 410 nm, very similar as in the spectrum of the product of the reaction of these Mn complexes with Ce(IV).[107] The brown solution produced a solid with no organic groups visible in IR spectrum after evaporation of water.

The reaction of Ce(IV) with Mn(II) has been known and studied extensively. The results showed that an equilibrium between Mn(II), Mn(III), Ce(III) and Ce(IV) is attained in all the experiments:[29]

Mn(II) + Ce(IV) ↔ Mn(III) + Ce(III) Eq (1)

In a new EDX experiment, we found that the products of the reaction of many Mn complexes with Ce(IV) are $Ce_xMn(III)_{1-x}(NO_3)_3$, forming nano-sized particles. As shown in Fig. 10, only a few minutes after reaction with Ce(IV), a compound containing low amount of carbon and a high amount of nitrogen and oxygen forms, showing decomposition of the Mn complexes immediately after their reaction with Ce(IV) (Fig. 10). Increasing N in the decomposed product is related to attach $NH_4^+$ from Ce(IV) solution to clay (Fig. 10). The result is consistent with the previously reported data regarding $CO_2$ formation under these conditions by other Mn complex. No presence of the organic groups in FTIR spectra recorded for this compound is observed as Ce(IV) serves as a powerful oxidant to decompose of the organic ligands.

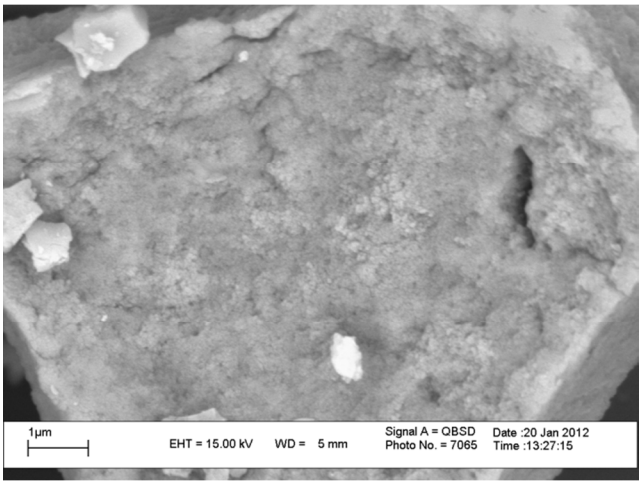


a

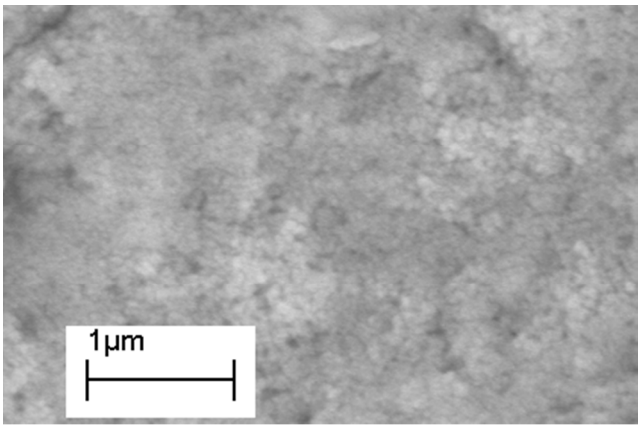


b

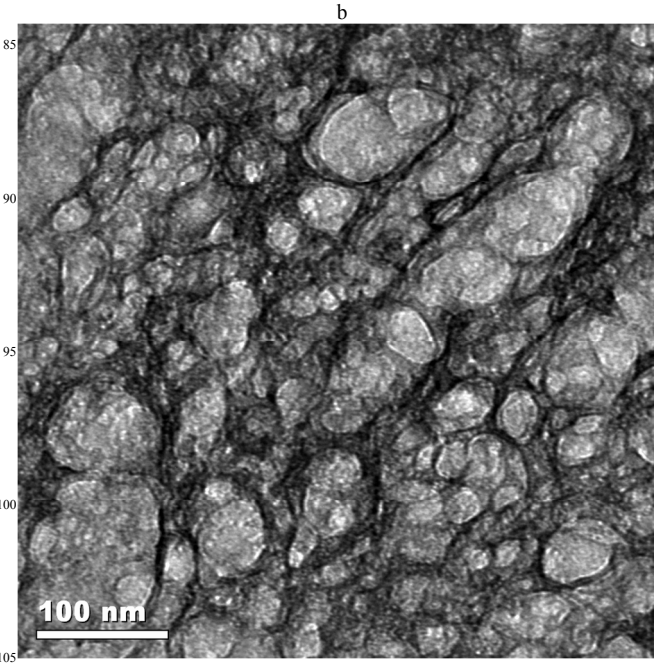


c

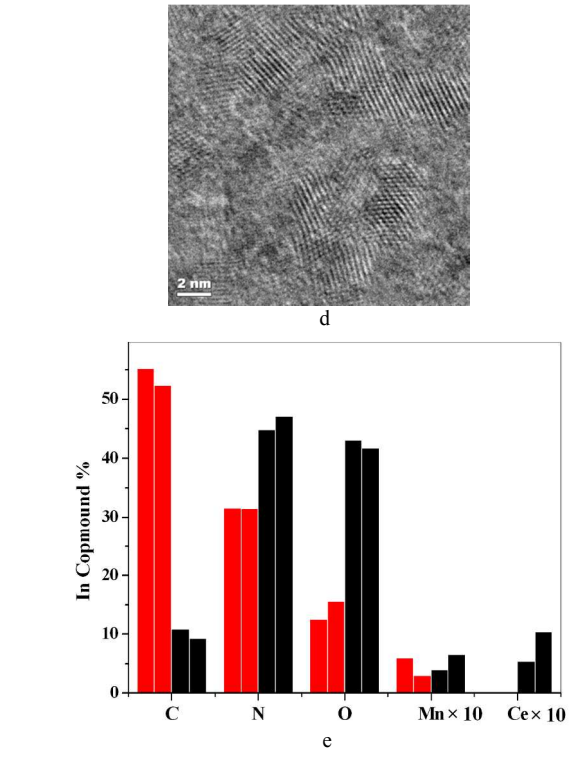


Fig. 10 SEM (a,b) and TEM (c,d) images after treating of **16** with Ce(IV) (0.5 M) and EDX (e) elemental analysis for **16** before (red) and after (black) reaction with Ce(IV) carried out for 10 minutes (0.5 M). Two points before and after treating with Ce(IV) were selected and elemental analysis was carried out.

It is important to note that the rate of oxygen evolution catalysed by Mn oxides prepared in the decomposition of Mn complexes may be different from the rate of oxygen evolution by usual Mn oxides, because organic compounds formed in decomposition of the ligands around the Mn oxides may increase the water-oxidizing activity.[106c,107,110-112] The Chang and Spiccia groups recently using TEM and electron scattering simulations results related the efficiency of formed Mn oxide in the presence of organic compounds to high degree of layer mis-registration, and Mn vacancies, compared to other Mn oxides.[112]

We also found that in the presence of Oxone, only Mn complexes with carboxylate groups decompose to $MnO_4^-$ but in the presence of Ce(IV) all Mn complexes decompose to $MnO_4^-$.

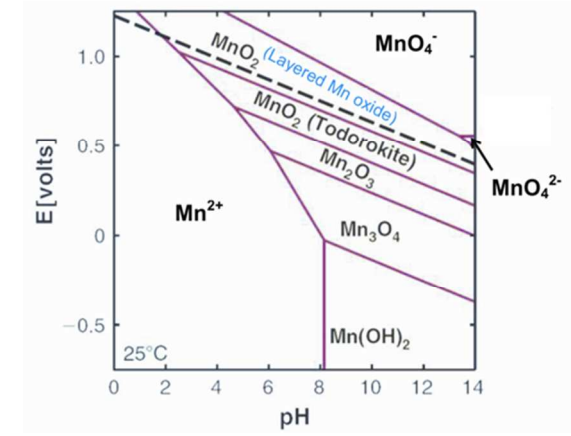


Scheme 3 Pourbaix diagrams for Mn. Layered Mn oxide is the most stable Mn oxide at high enough potential with modification from ref. 113.

Recently, $[(OH_2)(terpy)Mn(\mu\text{-}O)_2Mn(terpy)(OH_2)]^{3+}$-montmorillonite in the presence of Ce(IV) was considered by EXAFS.[110] This reaction is very interesting as the system is a model for the OEC in PSII.[114] The groups showed that after treating with Ce(IV) (0.25 M):[110] Regarding EXAFS and XANES data, it was found that after treatment with Ce(IV), the simulation results for the $[(OH_2)(terpy)Mn(\mu\text{-}O)_2Mn(terpy)(OH_2)]^{3+}$-montmorillonite hybrid material show a clear transformation to a layered oxide structure.[110] The results show that a Mn oxide formation-process before water oxidation occurs for the complex adsorbed on montmorillonite.

All of these results show that a Mn oxide with low amounts of carbon and nitrogen is formed on montmorillonite and that this compound is able to oxidize water.[110] As Mn oxides are efficient catalysts for water oxidation, thus the nano-sized Mn oxides were proposed as active catalysts in the reaction of the complex and Ce(IV). Thus, it seems that Mn oxides are the most important and stable Mn-based catalysts toward water oxidation.

## Conclusions

Results from our and other groups show that many Mn complexes electrochemically or chemically decompose to Mn oxides, and then these active Mn oxides oxidize water. In many of these experiments a layered Mn oxide is detected as the true catalyst for water oxidation. Regarding Pourbaix diagram, we also propose that a layered structure is the most stable phase under these conditions. More interestingly, it was shown that many Mn oxides under high oxidizing power convert to the layered Mn oxide.[115] Scheme 4 shows a summary of the proposed mechanisms for water oxidation by Mn-based catalysts.

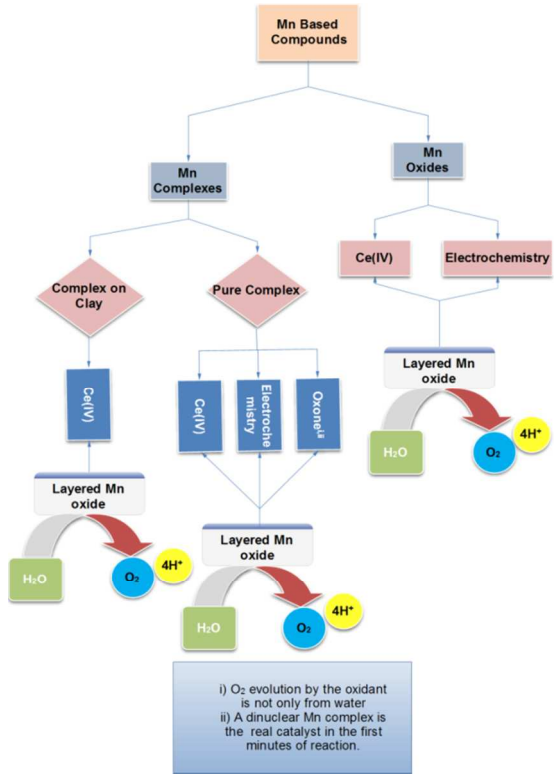

Scheme 4 In many oxygen evolution reactions catalyzed by Mn-based compounds, a layered Mn oxide is the true catalyst. *In the case of Oxone as oxidant, other intermediates than Mn oxides are also present. In the case of this oxidant in the presence of Mn oxide, oxygen evolution and not water oxidation occurs.

The authors are grateful to the Institute for Advanced Studies in Basic Sciences, the National Elite Foundation, Philipps-Universität Marburg, University of Mohaghegh Ardabili and Research School of Biology in Canberra for financial support. The image in Fig. 1a was made with VMD software and is owned by the Theoretical and Computational Biophysics Group, NIH Resource for Macromolecular Modeling and Bioinformatics, at the Beckman Institute, University of Illinois at Urbana-Champaign. The original data for the image are taken from ref. 2 (PDB: 3ARC)

## Notes and references

[a] *Department of Chemistry, Institute for Advanced Studies in Basic Sciences (IASBS), Zanjan 45137-66731, Iran*
[b] *Center of Climate Change and Global Warming, Institute for Advanced Studies in Basic Sciences (IASBS), Iran.*
[c] *Fachbereich Chemie and Wissenschaftliches Zentrum für Materialwissenschaften (WZMW), Philipps-Universität Marburg, Hans-Meerwein-Straße, D-35032 Marburg, Germany*
[d] *Department of Applied Chemistry, Faculty of Sciences, University of Mohaghegh Ardabili, Ardabil, P. O. Box: 56199-11367, Iran.*
[e] *Research School of Biology, Canberra, ACT 0200, Australia*
**Corresponding author. E-mail address: mmnajafpour@iasbs.ac.ir (M.M. Najafpour);Tel.: +98 241 4153201; Fax.: +98 241 4153232*;
† Electronic Supplementary Information (ESI) available: [details of any supplementary information available should be included here]. See DOI: 10.1039/b000000x/
‡These authors contributed equally to the work.
‖ This article is dedicated to the memory of Dr. Warwick Hillier who died on January 10, 2014.

1 K. N. Ferreira, T. M. Iverson, K. Maghlaoui, J. Barber and S. Iwata, *Science*, 2004, **303**, 1831.
2 Y. Umena, K. Kawakami, J.-R. Shen and N. Kamiya, *Nature*, 2011, **473**, 55.
3 M. M. Najafpour, A. Nemati Moghaddam, Y. N. Yang, E. Aro, R. Carpentier, J. J. Eaton-Rye, C. Lee and S. I. Allakhverdiev, *Photosynth. Res*., 2012, **114**, 1.
4 H. Wariishi, V. Khadar and M. H. Gold, *Biochemistry*, 1989, 28, 6017.
5 R. Cammack, A. Chapman, W. P. Lu, A. Karagouni and D. P. Kelly, *FEBS Lett*., 1989, **253**, 239.
6 V. Barynin, M. Whittaker, S. Antonyuk, V. Lamzin, P. Harrison, P. Artymiuk and J. Whittaker, *Structure*, 2001, **9**, 725.
7 P. Nordlund, B. M. Sjoberg and H. Eklund, *Nature*, 1990, **345**, 593.
8 Y. Sugiura, H. Kawabe, H. Tanaka, S. Fujimoto and A. Ohara, *J. Biol. Chem*., 1981, **256**, 10664.
9 W. C. Stallings, K. A. Pattridge, R. K. Strong and M. L. Ludwig, *J. Biol. Chem.*, 1985, 260, 16424.
10 N. S. Lewis and D. G. Nocera, *Proc. Natl. Acad. Sci. USA*, 2007, **104**, 20142; M. M. Najafpour, A. Nemati Moghaddam, S. I. Allakhverdiev and Govindjee, *Biochim. Biophys. Acta,* 2012, **1817**, 1110; M. M. Najafpour and Govindjee, *Dalton Trans*., 2011, **40**, 9076; R. Pace, An Integrated Artificial Photosynthesis Model. In: A. F. Collings, C. Critchley (eds), Artificial photosynthesis: From basic biology to industrial application, First Edn., Wiley-VCH, Weinheim (2005), pp 13-34; H. Dau and I. Zaharieva, *Acc. Chem. Res*., 2009, **42**, 1861; M. Wiechen, M. M. Najafpour, S. I. Allakhverdiev and L. Spiccia, *Energy Environ. Sci*., 2014, DOI: 10.1039/C4EE00681J.
11 X. Liu and F. Wang, *Coord. Chem. Rev*., 2012, **256**, 1115.
12 M. M. Najafpour and S. I. Allakhverdiev, *Int. J. Hydrogen Energy*, 2012, **37**, 8753; P. Kurz, G. Berggren, M. F. Anderlund and S. Styring, *Dalton Trans*., 2007, 4258; P. Kurz, *Dalton Trans*., 2009, 6103; R. Brimblecombe, G. F. Swiegers, G. C. Dismukes and L. Spiccia, *Angew. Chem. Int. Ed., 2008,* **120**, 7445; W. Ruettinger and G. C. Dismukes, *Chem. Rev., 1997,* **97**, 1; M. Yagi and M. Kaneko, *Chem. Rev.,* 2001, **101**, 21; C. W. Cady, R. H. Crabtree and G. W. Brudvig, *Coord. Chem. Rev*., 2008, **252**, 444; B. Conlan, N. Cox, J. Su, W. Hillier, J. Messinger, W. Lubitz, P. L. Dutton and T. Wydrzynski, *Biochim. Biophys. Acta*, 2009, **1787**, 1112; M. M. Najafpour, B. Kozlevcar, V. McKee, Z. Jaglicic and M. Jagodic, *Inorg. Chem. Commun.*, 2011, **14** (1), 125; L. Chou, R. Liu, Wanshu He, N. Geh, Y. Lin, E. Y. F. Hou, D. Wang and H. J. M. Hou, *Int. J. Hydrogen Energy*, 2012, **37**, 8889; H. J. M. Hou, *Materials*, 2011, **4**, 1693; R. Liu, Y. Lin, L. Chou, S. W. Sheehan, W. He, F. Zhang, H. J.M. Hou and D. Wang, *Angew. Chem. Int. Ed*., 2011, **50**, 499; F. Zhang, C. W. Cady, G. W. Brudvig, and H. J. M. Hou, *Inorg. Chim. Acta*, 2011, **366**, 128.
13 E. A. Karlsson, B. Lee, T. Åkermark, E. V. Johnston, M. D. Krks, J. Sun, O. Hansson, J. Bckvall and B. Åkermark, *Angew. Chem. Int. Ed.*, 2011, **50**, 11715.
14 J. Limburg, J. S.Vrettos, L. M. Liable-Sands, A. L. Rheingold, R. H. Crabtree and G. W. Brudvig, *Science,* 1999, **283**, 1524.
15 T. S. Glikman and I. S. Shcheglova, *Kinetika i Kataliz*. **1968**, 9, 461. V. Y. Shafirovich and A. E. Shilov, *Kinetika i Kataliz (translated from Russian)* 1979, 20, 1156; M. Morita, C. Iwakura and H. Tamura, *Electrochim. Acta*, 1977, **22**, 325; A. Harriman, I. J. Pickering, J. M. Thomas and P. A. Christensen, *J. Chem. Soc., Faraday Trans*. 1 1988, **84**, 2795; M. M. Najafpour, F. Rahimi, E. Aro, C. Lee and S. I. Allakhverdiev, *J. R. Soc. Interface* 2012, **9**, 2383; M. M. Najafpour, *Origins Life Evol. Biosph*., 2011, **41**, 237; M. M. Najafpour, *Geomicrobiol. J*., 2011, **28**, 714; M. M. Najafpour, F. Rahimi, M. Fathollahzadeh, B. Haghighi, M. Hołyńska, T. Tomo and S. I. Allakhverdiev, Dalton Trans., 2014, DOI: 10.1039/C4DT01295J; M. M. Najafpour, M. Amouzadeh Tabrizi, B. Haghighi and Govindjee, *Dalton Trans.,* 2012, **41**, 3906; M. M. Najafpour, M. Amouzadeh Tabrizi, B. Haghighi and Govindjee, *Dalton Trans.,* 2013, **42**, 879; M. M. Najafpour, *Chem. Commun*., 2011, **47**, 11724; M. M. Najafpour, *J. Photochem. Photobiol. B*, 2011, **104**, 111; M. M. Najafpour, D. Jafarian Sedigh, C. K. King'ondu and S. L. Suib, *RSC Adv*., 2012, **2**, 11253; M. M. Najafpour and A. Nemati Moghaddam, *New. J. Chem*., 2012, **36**, 2514; F. Zhou, A. Izgorodin, R. K. Hocking, V. Armel, L. Spiccia and D. R. MacFarlane, *ChemSusChem*, 2013, **6**, 643; M. M. Najafpour, T. Ehrenberg, M. Wiechen and P. Kurz, *Angew. Chem., Int. Ed*. 2010, **49**, 2233.
16 F. Jensen, *Introduction to Computational Chemistry*, John-Wiley Ltd, 2nd Ed. Chichester, England, 2007.
17 J. Yano, J. Robblee, Y. Pushkar, M. A. Marcus, J. Bendix, J. M. Workman, T. J. Collins, E. I. Solomon, S. D. George and V. K. Yachandra, *J. Am. Chem. Soc.*, 2007, **129**, 12989.
18 E. M. Sproviero, J. P. McEvoy, J. A. Gasco´n, G. W. Brudvig and V. S. Batista, *Photosynth. Res.*, 2008, **97**, 91.
19 D. A. Pantazis, M. Orio, T. Petrenko, S. Zein, W. Lubitz, J. Messinger and F. Neese, *Phys. Chem. Chem. Phys.*, 2009, **11**, 6788.
20 P. E. M. Siegbahn, *Acc. Chem. Res.*, 2009, **42**, 1871.
21 T. Wang, G. Brudvig, and V. S. Batista, *J. Chem. Theory Comput.*, 2010, **6**, 755.
22 N. Cox, L. Rapatskiy, J.-H. Su, D. A. Pantazis, M. Sugiura, L. Kulik, P. Dorlet, A. W. Rutherford, F. Neese, A. Boussac, W. Lubitz and J. Messinger, *J. Am. Chem. Soc.*, 2011, **133**, 3635.
23 M. Busch, E. Ahlberg and I. Panas, *Phys. Chem. Chem. Phys.*, 2011, **13**, 15069.
24 S. Luber, I. Rivalta, Y. Umena, K. Kawakami, J.- R. Shen, N. Kamiya, G. W. Brudvig and V. S. Batista, *Biochemistry*, 2011, **50**, 6308.
25 P. E. M. Siegbahn, *ChemPhysChem*, 2011, **12**, 3274.
26 Y. Gao, R. H. Crabtree and G. W. Brudvig, *Inorg. Chem.*, 2012, **51**, 4043.
27 A. Grundmeier and H. Dau, *Biochim. Biophys. Acta*, 2012, **1817**, 88.
28 P. E. M. Siegbahn, *Phys. Chem. Chem. Phys.*, 2012, **14**, 4849.
29 A. D. Becke, *J. Chem. Phys.*,1993, **98**, 5648.
30 T. H. Dunning Jr. and P. J. Hay, in *Modern Theoretical Chemistry*, Ed. H. F. Schaefer III, Vol. 3 (Plenum, New York, 1976) 1-28.
31 P. J. Hay and W. R. Wadt, *J. Chem. Phys.*,1985, **82**, 270.
32 P. J. Hay and W. R. Wadt, *J. Chem. Phys.*,1985, **82**, 299.
33 G. M. Sheldrick, SHELXTL 5.1, Bruker AXS Inc., 6300 Enterprise Lane, Madison, WI 53719-1173, USA, 1997.

34 Y. Li, M. Wang, L.Wang and C.Xia, *Acta Cryst. C*, 2000, **56**, 445; B. Figgis, C. L. Raston, R. Sharma and A. H. White, *Aust. J. Chem*., 1978, **31**, 2545.

35 W. B. Lin, M. E. Chapman, Z. Y. Wang, G. T. Yee, *Inorg. Chem.*, 2000, **39**, 4169.

36 I. Hwang and K. Ha, *Acta Crystallogr E*., 2006, **E62**, m376.

37 W. Wang, C. Ma, F. Chen, C. Chen and Q. Liu, *Acta Crystallogr. E,* 2003, **E62**, m908.

38 C. Ma, F. Chen, X. Zhang, C.Chen and Q Liu, *Acta Crystallogr. C*, 2002, **C58**, m401.

39 D. M. Boghaei and M. M. Najafpour, *Anal. Sci., X-ray Structure Analysis*, 2008, **23**, x123.

40 J. Zou, Z. Xu, , W. Chen, K. M. Lo and X. You, *Polyhedron*, 1999, **18**, 1507.

41 M. Devereux, M. Jackman, M. McCann and M. Casey, *Polyhedron*, 1998, **17**, 153.

42 Solubility of **10** and **13** in water is low.

43 C. Ma, F. Chen, C. Chen and Q. Liu, *Acta Cryst. C*, 2003, **C59**, m516.

44 M. M. Najafpour, M. Amini, M. Bagherzadeh, D. M. Boghaei and V. McKee, *Trans. Met. Chem*., 2010, **35**, 297.

45 M. D. Wodrich, C. Corminboeuf and P. von R. Schleyer, *Org. Lett.*, 2006, **8**, 3631.

46 A. A. Granovsky, Firefly version 8.0.0: http://classic.chem.msu.su/gran/firefly/index.html

47 M. W. Schmidt, K. K. Baldridge, J. A. Boatz, S. T. Elbert, M. S. Gordon, J. H. Jensen, S. Koseki, N. Matsunaga, K. A. Nguyen, S. Su, T. L. Windus, M. Dupuis and J. A. Montgomery, *J. Comput. Chem.*, 1993, **14**, 1347.

48 CSD database, ver. 5.34, November 2012.

49 W. Henke, S. Kremer and D. Reinen, *Z. Anorg. Allg. Chem*., 1989, **491**, 124.

50 E. N. Maslen, C. L. Raston and A. H. White, *J. Chem. Soc., Dalton Trans.*, 1975, 323.

51 Chin-Wing Chan, Chi-ming Che and Shie-Ming Peng, *Polyhedron*, 1993, **12**, 2169.

52 (a) E. C. Constable, S. M. Elder, J. Healy, M. D. Ward and D. A. Tocher, *J. Am. Chem. Soc.*, 1990, **112**, 4590; (b) E. C. Constable, S. M. Elder, M. J. Hannon, A. Martin, P. R. Raithby and D. A. Tocher, *J. Chem. Soc., Dalton Trans*., 1996, 2423.

53 C. Che, Y. Wang, K. Yeung, K. Wong and S. Peng, *J. Chem. Soc., Dalton Trans*., 1992, 2675.

54 (a) C. Che, C. Chan, S. Yang, C. Guo, C. Lee and S. Peng, *J. Chem. Soc., Dalton Trans*., 1995, 2961; (b) D. B. Dell' Amico, F. Calderazzo, U. Englert, L. Labella and F. Marchetti, *J. Chem. Soc., Dalton Trans*., 2001, 357.

55 C. Chan, C. Che, M. Cheng and Y. Wang, *Inorg. Chem*., 1992, **31**, 4874.

56 D. B. Dell'Amico, F. Calderazzo, M. Curiardi, L. Labella and F. Marchetti, *Inorg. Chem. Commun*., 2005, **8**, 673.

57 D. B. Dell'Amico, F. Calderazzo, M. Curiardi, L. Labella and F. Marchetti, *Inorg. Chem*., 2004, **43**, 5459.

58 E. C. Constable, S. M. Elder, M. J. Hannon, A. Martin, P. R. Raithby and D. A. Tocher, *J. Chem. Soc., Dalton Trans*., 1996, 2423.

59 E. C. Constable, S. M. Elder and D. A. Tocher, *Polyhedron*, 1992, **11**, 2599.

60 San-Ming Yang, Kung-Kai Cheung, Chi-Ming Che *J. Chem. Soc., Dalton Trans*., 1993, 3515.

61 (a) C. Che, C. Chan, S. Yang, C. Guo, C. Lee and S. Peng, *J. Chem. Soc., Dalton Trans*., 1995, 2961; (b) F. Calderazzo, L. Labella and F. Marchetti, J. Chem. Soc., *Dalton Trans*., 1998, 1485.

62 D. Xiao, Y. Hou, E. Wang, J. Lu, Y. Li, L. Xu and C. Hu, *Inorg. Chem. Commun*., 2004, **7**, 437.

63 M. Barboiu and J. -M. Lehn, *Rev. Chim.* (Bucharest Rom.), 2006, **57**, 909.

64 C. W. Cady, C. Incarvito, G. W. Brudvig and R. H. Crabtree, *Inorg. Chim. Acta*, 2006, **359**, 2509.

65 G. Zhang, X. Zhang and G. Yu, *Acta Cryst. E*, 2008, **E64**, m214.

66 B. C. Polander and B. A. Barry, *Proc. Natl. Acad. Sci. USA*, 2012, **109**, 6112.

67 P. King, R. Clérac, C. E. Anson and A. K. Powell, *Dalton Trans*., 2004, 852.

68 L. Pan, N. Ching, X. Huang and J. Li, *Chem. -Eur. J*., 2001, **7**, 4431;

69 R. Sarma and J. B. Baruah, *Inorg. Chim. Acta*, 2011, **377**, 50.

70 P. King, R. Clérac, C. E. Anson and A. K. Powell, *Dalton Trans*., 2004, 852.

71 J. Tian, S. Yan, D. Liao, Z. Jiang and P. Cheng, *Inorg. Chem. Commun*., 2003, **6**, 1025.

72 R. G. Inskeep. *J. Inorg. Nucl. Chem*., 1996, **28**, 2285.

73 K. Nakamoto, Infrared and Raman Spectra of Inorganic and Coordination Compounds, fourth edition, A Wiley-Interscience Publication, 1986.

74 A. Majumder, C. R. Choudhury, S. Mitra, C. Marschner and J. Baumgartner, *Z. Naturforsch*., 2005, **60b**, 99.

75 A. Majumder, G. Pilet, M.Teresa G. Rodriguez and S. Mitra, *Polyhedron*, 2006, **25**, 2550.

76 C. Zscherp and A. Barth, *Biochemistry,* 2001, **47**, 1875.

77 D. H. R. Barton, S. D. Be`vie`re, W. Chavasiri, D. Doller, W. G. Liu and J. H. Reibenspies, *New J. Chem*., 1992, **16**, 1019.

78 S. C. Chang, J. K. H. Ma, J. T. Wang and N. C. Li, *J. Coord. Chem*., 1972, **2**, 31-34.

79 R. Dingle and R. Aria, *Chem. Scand*., 1966, **20**, 33.

80 I. Kani, C. Darak, O. Sahin and O. Buyukgungor, *Polyhedron*, 2008, **27**, 1238.

81 F. E. Mabbs and D. Collison, Electron Paramagnetic Resonance of d Transition Metal Compounds, Elsevier, Amsterdam, 1992.

82 S.T. Warzeska, F. Micciche, M. C. Mimmi, E. Bouwman, H. Kooijman, A. L. Spek and J. Reedijk, *J. Chem. Soc. Dalton. Trans*., 2001, 3507.

83 E. Garribba, G. Micera and M. Zema, *Inorg. Chim. Acta* 2004, **357**, 2038.

84 C. R. Byfleet, W. C. Lin and C. A. McDowell, *Mol. Phys.*, 1970, **18**, 363.

85 M. M. Morrison and D.T. Sawyer, *Inorg. Chem.*, 1978, **17**, 338.

86 P. Kurz, M.F. Anderlund, N. Shaikh, S. Styring and P. Huang, *Eur. J. Inorg. Chem*., 2008, 762.

87 J. Limburg, G. W. Brudvig and R. H. Crabtree, *J. Am. Chem. Soc*., 1997, **119**, 2761;

88 B. Zeng, X. Zhu, X. Yu, S. Cai and Z. Chen, *Spectrochim. Acta Part A*, 2008, **69**, 117.

89 Z. Chen, Y. Wu, F. Huang, D. Gu and F. Gan, *Spectrochim. Acta Part A*, 2007, **66**, 1024.

90 X. Yu and S. Cai, Z. Chen, *Spectrochim. Acta Part A*, 2004, **60**, 391.

91 P. Sjöberg and D. M. Boghaei, *Spectrochim. Acta Part A,* 2010, **75**, 1168.

92 R. Tagore, R. H. Crabtree and G. W. Brudvig, *Inorg. Chem*., 2008, **47**, 1815.

93 L. Konerman, J. Messinger and W. Hillier, Mass Spectrometry-Based Methods for Studying Kinetics and Dynamics in Biological Systems. In (T. Matysik and T. Aartsma eds.) Biophysical Techniques in Photosynthesis Research II. Springer, 2008, pp. 167-190. [ISBN-10 1-4020-8249-5].

94 K. Beckman, J. Messinger, M.R. Badger, T. Wydrzynski and W. Hillier, *Photosynth. Res*., 2009, **102**, 511.

95 K. Beckmann, H. Uchtenhagen, G. Berggren, M. F. Anderlund, A. Thapper, J. Messinger, S. Styring and P. Kurz, *Energy Environ. Sci*., 2008, **1**, 668;

96 a) J. Limburg, J. S. Vrettos, H. Y. Chen, J. C. de Paula, R. H. Crabtree and G. W. Brudvig, *J. Am. Chem. Soc*., 2001, **123**, 423. b) M. M. Najafpour, D. M. Boghaei and V. McKeec, *Polyhedron*, 2010, **29**, 3246.

97 D. Shevela, S. Koroidov, M. M. Najafpour, J. Messinger and P. Kurz, *Chem. Eur. J*., 2011, **17**, 5415.

98 Z. Zhang, J. O. Edwards and P. H. Rieger, *Inorg. Chim. Acta*, 1994, **221**, 25.

99 M.M. Morrison and D.T. Sawyer, *Inorg. Chem*., 1978, **17**, 333.

100 C. Baffert, S. Dumas, J. Chauvin, J. C. Lepreˆtre, M. N. Collomb and A. Deronzier, *Phys. Chem. Chem. Phys*., 2005, **7**, 202.

101 M. N. Collomb, D. Sauthier, A. Deronzier and X. Pradon, *J. Am. Chem. Soc*., 1997, **119**, 3173.

102 M. N. Collomb, D. Sauthier, A. Deronzier, A. Piron, X. Pradon and S. Me´nage, *J. Am. Chem. Soc*., 1998, **120**, 5373.

103 M. Kasuno, M. Hayano, M. Fujiwara and T. Matsushita, *Polyhedron*, 2009, **28**, 425.

104 Y. Kozlov, A. A. Kazakova and V. V. Klimov, *Membr. Cell Biol.* 1997, **11**,115.
105 W. -H. Kao and V. J. Weibel, *J. Applied Electrochem.*, 1992, **22**, 21.
106 a) R. K. Hocking, R. Brimblecombe, L. Chang, A. Singh, M. H. Cheah, C. Glover, W. H. Casey and L. Spiccia, *Nat. Chem*. 2011, **3**, 461.
b) R. Brimblecombe, G. F. Swiegers, G. C. Dismukes and L. Spiccia, *Angew. Chem. Int. Ed.*, 2008, **47**, 7335.
c) A. Singh, R. K. Hocking, S. L. Y. Chang, B. M. George, M. Fehr, L. Klaus, A. Schnegg and L. Spiccia, *Chem. Mater.*, 2013, **25**, 1098.
d) M. M. Najafpour, B. Haghighi, M. Zarei Ghobadia and D. Jafarian Sedigha, Chem. Commun., 2013, **49**, 8824.
107 M. M. Najafpour and A. Nemati Moghaddam, *Dalton Trans*. 2012, **41**, 10292.
108 D. Ramalakshmi and M. V. Rajasekharan, *Acta Cryst. B*, 1999, **B55**, 186.
109 K. R. Reddy, M. V. Rajasekharan, N. Arulsamy and D. J. Hodgson, *Inorg. Chem*. 1996, **35**, 2283.
110 M. M. Najafpour, A. Nemati Moghaddam, H. Dau, I. Zaharieva, *J. Am. Chem. Soc*., 2014, **136**, 7245.
111 T. Takashima, K. Hashimoto and R. Nakamura, *J. Am. Chem. Soc.,* 2012, **134**, 18153.
112 S. L. Y. Chang, A. Singh, R. K. Hocking, C. Dwyer and L. Spiccia, *J. Mater. Chem. A*, 2014, **2**, 3730.
113 A. Izgorodin, O. Winther-Jensen and D. R. MacFarlane, *Aust. J. Chem.* 2012, **65**, 638.
114 M. Yagi and K. Narita, *J. Am. Chem. Soc.*, 2004, **126**, 8084; K. Narita, T. Kuwabara, K. Sone, K. Shimizu and M. Yagi, *J. Phys. Chem. B*, 2006, **110**, 23107; M. Yagi, K. Narita, Maruyama, K. Sone, T. Kuwabara and K. Shimizu, *Biochim. Biophys. Acta-Bioenerg.*, 2007, **1767**, 660; M. Wiechen, H. Berends and P. Kurz*, Dalton Trans.,* 2012*,* **41**, 21; H. M. Berends, T. Homburg, I. Kunz and P. Kurz, *Appl. Clay Sci*., 2011, **53**, 174*;* P. Kurz, *Dalton Trans.*, 2009, 6103.
115 M. M. Najafpour and D. Jafarian Sedigh, *Dalton. Trans*., 2013, **42**, 12173; M. M. Najafpour, B. Haghighi, D. Jafarian Sedigh and M. Zarei Ghobadi, *Dalton Trans*., 2013, **42**, 16683.